Accepted Manuscript

Dynamic mass based sound transmission loss prediction of vibro-acoustic metamaterial double panels applied to the mass-air-mass resonance

N.G.R. de Melo Filho, L. Van Belle, C. Claeys, E. Deckers, W. Desmet

PII: S0022-460X(18)30727-2

DOI: https://doi.org/10.1016/j.jsv.2018.10.047

Reference: YJSVI 14464

To appear in: *Journal of Sound and Vibration*

Received Date: 24 May 2018

Revised Date: 2 October 2018

Accepted Date: 25 October 2018

Please cite this article as: N.G.R. de Melo Filho, L. Van Belle, C. Claeys, E. Deckers, W. Desmet, Dynamic mass based sound transmission loss prediction of vibro-acoustic metamaterial double panels applied to the mass-air-mass resonance, *Journal of Sound and Vibration* (2018), doi: https://doi.org/10.1016/j.jsv.2018.10.047.

Dynamic mass based sound transmission loss prediction of vibro-acoustic metamaterial double panels applied to the mass-air-mass resonance

N. G. R. de Melo Filho[a,b], L. Van Belle[a,b], C. Claeys[a,b], E. Deckers[a,b], W. Desmet[a,b]

[a] *KU Leuven, Department of Mechanical Engineering, Division PMA*
Celestijnenlaan 300-box 2420, 3001 Heverlee, Belgium
[b] *DMMS lab, Flanders Make*

Abstract

To enhance the sound insulation performance of double panel partitions at their mass-air-mass resonance frequency, novel compact and low-mass solutions are sought. This paper investigates the use of the locally resonant vibro-acoustic metamaterial concept as a possible solution. The metamaterial solution is applied to one panel of a double panel partition in order to enhance the sound transmission loss at the mass-air-mass resonance. To design the metamaterial solution and predict its sound transmission loss performance, an extension of the multiple reflection theory is proposed, incorporating the dynamic mass of a metamaterial panel. The latter is obtained from the metamaterial plate dispersion curves, calculated using finite element based unit cell modeling. The designed metamaterial solution is manufactured and its insertion loss is measured. The novel design outperforms the original double panel and an equivalent total mass double panel configuration in the targeted mass-air-mass resonance frequency region. The predictions obtained with the proposed method are in good agreement with the experimentally obtained results. This demonstrates the

Nomenclature

α	Factor to adjust measured and predicted STL
ΔIL	IL difference between metamaterial and bare structure [dB]
$*^{(red)}$	Reduced matrix or vector $*$
$\mathbf{f}$	Nodal force vector
$\mathbf{K}$	Stiffness matrix
$\mathbf{k}$	Wave vector
$\mathbf{M}$	Mass matrix
$\mathbf{q}$	Generalized displacement vector
$\mathbf{R}$	Matrix representing the phase shift relationship
μ_i	Propagation constant along lattice vector d_i
ω	Angular frequency [rad/s]
ω_2	Natural frequency of the second DOF of the 2 DOF system
ω_β	Upper frequency limit of the negative dynamic mass region
ω_H	Upper frequency limit of the stop band [rad/s]
ω_L	Lower frequency limit of the stop band [rad/s]
$\overline{\tau}$	Diffuse field transmission coefficient
$\overline{f}$	Averaged natural frequency [Hz]
Φ_i	Amplitude of the incident wave
Φ_t	Amplitude of the transmitted wave
ρ_0	Air density [kg/m^3]
σ	Standard deviation
τ	Transmission coefficient
τ_i	Mass-law of the panel i
θ	Angle of incidence of the acoustic ray
θ_l	Maximum angle of acoustic plane wave incidence
$\tilde{m}$	Dynamic mass [kg]
$\tilde{u}_1$	Displacement of the 1 DOF system with dynamic mass
$\tilde{X}_1$	Mode shape of the 1 DOF system with dynamic mass
ζ_2	Modal damping ration
$*^T$	Conjugate transpose
c_0	Speed of sound in air [m/s]
c_2	Damping coefficient [N/m/s]
d	Air gap thickness [m]
d_i	Lattice vector in the direction i
F_0	Force [N]
f_i	Measured natural frequency of the resonant structure i [Hz]
f_{MAM}	Mass-air-mass resonance frequency [Hz]
IL	Sound insertion loss [dB]
IL_B	Measured IL of the bare double panel [dB]
IL_M	Measured IL of the metamaterial double panel [dB]
j^2	-1
k	Wavenumber of air
k_2	Spring stiffness [N/m]
m_i'	Mass per area of panel i [kg/m^2]
m_*	Mass of the * DOF of the 2 DOF system [kg]
m_{HS}	Mass of the host structure [kg]
m_{Res}	Mass of the resonant structure [kg]
n	Number of tested resonant structures
t	Time [s]
u_*	Displacement of the * DOF of the 2 DOF system
W	Measured sound power [W]
X_1	Mode shape of the first DOF of the 2 DOF system

potential of the metamaterial solution to enhance the acoustic insulation at the mass-air-mass resonance and indicates that the proposed method allows a fast, simple and representative indication of their acoustic insulation performance.

Keywords: Locally resonant metamaterial, stop band, sound transmission loss, double panel partition, dynamic mass, mass-air-mass resonance

1. Introduction

Double panels partitions are widely used in building applications due to their low weight, good thermal insulation and high sound transmission loss (STL). These partitions outperform the acoustic mass-law of a single panel of the same mass in a large frequency range. However, a mass-air-mass resonance is created at which both panels resonate on the stiffness of the separating air layer, causing a frequency region of poor STL performance [1, 2, 3, 4]. The classical solutions for this vibro-acoustic problem are generally based on either adding mass or increasing the space between the panels. This leads to heavy and bulky structures, which is undesirable in the context of the current trend towards lightweight design.

Locally resonant metamaterials have recently come to the fore as potential novel lightweight solutions for vibro-acoustic problems, be it in a well-defined frequency ranges, referred to as stop bands [5, 6, 7, 8, 9, 10, 11, 12]. These are created by the addition of resonant structures to a host structure

*Corresponding author: noegeraldo.rochademelofilho@kuleuven.be

on a sub-wavelength scale, resulting in a tunable frequency region where no free waves can propagate due to a Fano-type interference between the resonant and host structure [5, 8, 13, 14]. The stop band frequency region can be predicted based on dispersion diagrams, which can be calculated by unit cell (UC) modeling using the finite element (FE) method in combination with the Bloch-Floquet theorem [15, 16, 17, 18]. It is known that stop bands lead to frequency regions with high vibration attenuation and high STL [6, 7, 19, 20]. Since the poor STL performance of a double panel partition caused by the mass-air-mass resonance is a vibro-acoustic problem in a well-defined frequency range, the locally resonant metamaterial concept is a potential solution [21, 22, 23, 24]. Consequently, in this work, the metamaterial concept is applied to a double panel partition by adapting one of both panels to a locally resonant metamaterial panel.

To predict the STL of a double panel partition with one metamaterial panel, some methods have been proposed in recent literature. In [21], the analytical formulation of a finite panel is coupled with mass-spring systems to derive the STL performance of a double panel partition. This does not allow the use of realizable resonant structures. In [22], the plane wave expansion is used to define an effective medium by the means of the dynamic mass of the metamaterial panel. The resonant structures are again treated as mass-spring systems and no experimental validation is shown. In [23], the acoustic mass-law is adapted to use the mass of the effective medium, a series of layers connected by springs, with added mass-spring resonators. Good agreement between model and experimental results are found, however, the method proposed again only considers mass-spring resonators and does consider complex resonant structure geometries. In [24], porous ma-

terial is introduced inside the air gap between both panels and different configurations of the double panel partition are studied. The porous material is modeled using Biot's theory and an equivalent fluid assumption. The resonant structures are again considered as mass-spring system and only numerical results are shown. In all of these works, only simple spring-mass resonators are considered instead of practically realisable geometries. Methods to predict the STL of infinite periodic structures with complex resonator geometries are also available. In [25], the UC is modeled using FE and the surrounding acoustic domain using the Wave Based method. Similarly, in [26], the FE UC model is coupled to the surrounding acoustic domain modeled using a plane wave expansion. The use of FE UC descriptions allows geometrically complex periodic structures to be considered. A last possibility is the use of full vibro-acoustically coupled FE models with Perfectly Matched Layer (PML) boundary conditions applied to the truncated acoustic domains, e.g. see [27, 28]. However, compared to simplified analytical representations, these FE based methods are computationally more expensive.

This paper proposes a simple method to estimate the STL performance of a double panel partition with a separating air gap, to which the metamaterial solution is applied with complex and realizable resonant structures. To achieve this, the Multiple Reflection Theory (MRT) [3] is applied as it shows an acceptable average error below ± 5 dB with experimental measurements for bare double panel partitions [29]. The MRT uses the acoustic mass law to predict the STL performance of a double panel partition. In order to incorporate the metamaterial stop band effect, the MRT is extend by including the dynamic mass of the metamaterial panel. The dynamic

mass of the metamaterial can be calculated using different approaches, often relying on the analytical equations of motion of a mass-spring system [30, 31, 32, 33]. In this paper, the equivalent dynamic mass is calculated by relating the stop band limits obtained from calculated dispersion curves for a metamaterial FE UC model to the negative mass frequency region of the metamaterial panel [34]. Doing so, the MRT extended with the dispersion curve based equivalent dynamic mass allows for computationally inexpensive and accurate STL predictions of metamaterial double panels with complex resonator geometries.

A realizable metamaterial design is proposed to enhance the STL around the mass-air-mass resonance frequency range of a double panel with a separating air gap. Its performance is predicted by the proposed extension of the MRT with the metamaterial dynamic equivalent mass. The potential of the metamaterial design and applicability of the prediction method are demonstrated by a comparison with experimental measurement results on a manufactured sample.

This paper is organized as follows. In section 2, the double panel and metamaterial design are defined. Section 3 describes the stop band prediction of undamped periodic structures and gives the stop band limits for the designed metamaterial panel. Section 4 introduces the dynamic mass based MRT method and the prediction and analysis of the STL performance of the considered configurations. In section 5, the experimental setup used to validate the resonant structure design and to measure the sound insertion loss is explained. The measured natural frequencies of the resonant structures and the measured sound insertion loss of the considered configurations are presented, analyzed and compared to numerical predictions in Section

6. Finally, section 7 summarizes the main findings of this work.

2. Problem definition

This section describes the double panel partition and introduces the metamaterial design to obtain stop band behavior around the bare double panel mass-air-mass resonance frequency range.

2.1. Double panel partition

The panels (and later also the resonant structures) are made of polymethyl methacrylate (PMMA). PMMA is chosen because of its light permeability, as this kind of partition is generally found in windows, where this characteristic is of great importance and needs to be preserved by the metamaterial solution. The material properties of PMMA are retrieved by weighing and model updating [35] of a PMMA panel with dimensions $300 \times 200 \times 4$ mm [7], taking into account all seven free-free modes below 500 Hz. After an updating of the material properties, the average mismatch between measured and numerically obtained natural frequencies is below 0.3%. The modal damping is estimated by the half power bandwidth method [36] as detailed in section 5.1. Table 1 shows the acquired material properties.

Table 1: Material properties of the PMMA used for the double panel partition and resonant structure.

Young's modulus	Poisson's ratio	Density	Modal Damping
4850 MPa	0.31	1188.38 kg/m^3	2.5%

The considered double panel configurations are composed of two PMMA panels of A2 dimensions (420×591 mm). The A2 area is chosen to guarantee a sufficiently high modal density of the panel in the frequency region of the mass-air-mass resonance, in order to reduce the influence of the panel modes on the STL, and corresponds to the wetted surfaces in the measurement setup introduced in section 5.

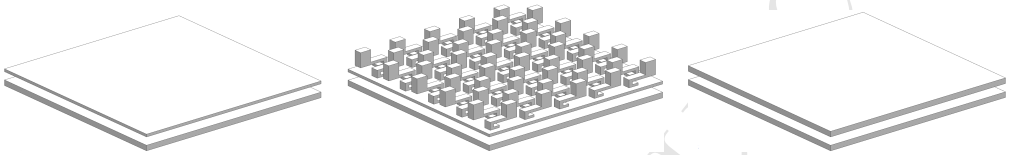

(a) (b) (c)

Figure 1: Schematic representation of the three configurations considered: (a) original, (b) metamaterial and (c) equivalent mass.

Three configurations are considered (Figure 1): original, metamaterial and equivalent mass double partitions. All configurations have an 8 mm air gap in between both panels. The original and metamaterial configurations are composed of two PMMA panels of 2 mm and 4 mm thickness. For the metamaterial configuration the 2 mm panel serves as the host structure. The equivalent mass configuration is composed of two 4 mm thick PMMA panels and has the same total static mass as the metamaterial configuration as will be discussed in section 2.2. The mass-air-mass resonance frequency f_{MAM} of the double panel partitions is calculated as [1]:

$$f_{MAM} = \frac{1}{2\pi}\sqrt{\left(\frac{\rho_0 c_0^2}{d}\right)\left(\frac{m_1' + m_2'}{m_1' m_2'}\right)}, \tag{1}$$

with ρ_0 the density of air, c_0 the speed of sound in air and m_1' and m_2' the

mass per area of each of the two panels. Corresponding to the ambient temperature $T = 20°\text{C}$ during the measurements, $\rho_0 = 1.225$ kg/m^3 and $c_0 = 340$ m/s are considered. The calculated mass-air-mass resonances for the configurations without resonant structures are listed in Table 2.

Table 2: Mass-air-mass resonance frequencies of the bare double panels with 8 mm air gap.

	Panels	f_{MAM}
Original	4 mm + 2 mm	532.9 Hz
Equivalent mass	4 mm + 4 mm	435.1 Hz

2.2. Metamaterial design

The metamaterial solution is designed to create a stop band in the frequency region around the mass-air-mass resonance frequency 532.9 Hz of the original double panel, targeting the flexural acoustically relevant waves. The host structure is the 2 mm thick panel and a mass addition of 100% with respect to this panel is aimed for, which results in a total mass addition of 33% with respect to the entire double panel.

To achieve stop band behavior, the resonant structures need to exert a non-zero net force on the structure with respect to the targeted out-of-plane bending motion [37] and need to be added on a sub-wavelength scale, smaller than half of the bending wavelength in the target frequency range [5]. A resonator consisting of a cantilever beam with an end-point mass meets the non-zero net force requirement at its first mode (Figure 2b), as demonstrated by the authors in [7, 38, 39].

By adapting the beam and mass dimensions, the resonator is tuned to the targeted mass addition and resonance frequency through manual iterations by evaluating its first bending mode using an FE model with 1010 linear solid elements and clamped base boundary conditions. In these iterations, the width of the resonators is fixed to 6 mm according to the PMMA panel thickness available for manufacturing by means of laser-cutting, while the PMMA material properties of Table 1 are used. Furthermore, to satisfy the sub-wavelength requirement, the resonant structures are added two by two in regular grid of 30 × 30 mm (Figure 3), determining their maximum size. The dimensions of the eventually fabricated resonator are shown in Figure 2a and are obtained by averaging the measured dimensions of 10 manufactured resonant structures.

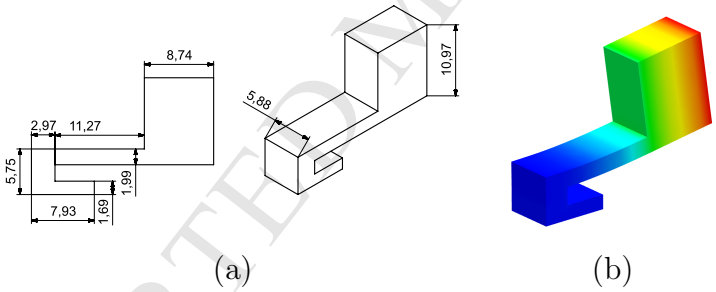

Figure 2: The manufactured resonator dimensions in mm obtained by averaging the measured dimensions of 10 manufactured resonators (a) and the resulting out-of-plane bending mode at 563 Hz (b) used to create a stop band.

3. Stop band prediction

This section briefly describes the UC modeling for stop band prediction. A more detailed description can be found in [5]. This section ends with the

stop band prediction of the designed metamaterial.

3.1. Unit cell modeling

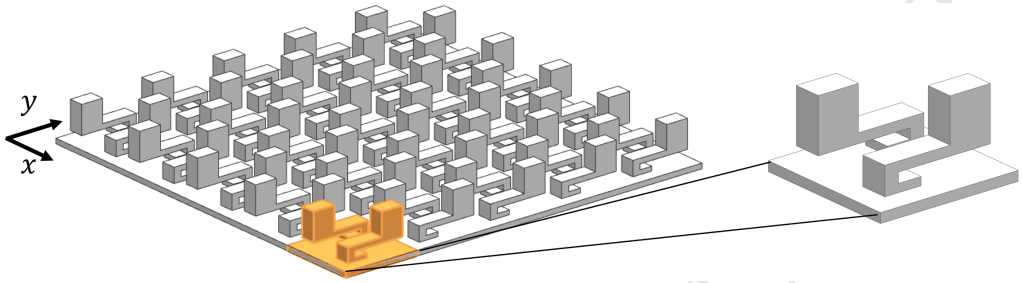

Figure 3: Periodic metamaterial (left) and its representative UC (right).

The often periodic configuration of locally resonant metamaterials is exploited in UC modeling to predict their stop band frequency range by analyzing dispersion diagrams, which describe the wave propagation in terms of wavenumber and frequency. They can be obtained by applying Bloch-Floquet periodicity boundary conditions to representative UC of the infinite periodic structure (Figure 3) and solving the resulting eigenvalue problem. In this work, the UC is modeled using FEM. This enables complex and realizable structures to be considered, while the small model size allows for fast stop band predictions.

As will be shown in section 4, the sound transmission loss predictions in this work will be based on the stop band limits of the metamaterial panel. In presence of damping, which is the case for the considered PMMA host structure and resonators, the notion of stop bands fades and transitions to a zone of increased wave attenuation, while the associated eigenvalue problem is more computationally expensive to solve [7, 38]. Hence, to allow fast and straightforward identification of the stop band limits, the wave propagation

in the undamped infinite periodic structure is assessed by calculating dispersion curves for the undamped structure. The FE equations of motion of an undamped UC are given by:

$$\left(\mathbf{K} - \omega^2 \mathbf{M}\right) \mathbf{q} = \mathbf{f}, \tag{2}$$

with $\mathbf{K}$ and $\mathbf{M}$ the stiffness and mass matrix respectively, ω the angular frequency, $\mathbf{q}$ the generalized displacement vector and $\mathbf{f}$ the generalized force vector.

The Bloch-Floquet theorem relates generalized displacements and forces on the UC boundary by using propagation factors $e^{j\mu_x}$ and $e^{j\mu_y}$, along the periodicity lattice vectors $\mathbf{d}_x$ and $\mathbf{d}_y$ (Figure 3), with $j^2 = -1$. The propagation constants μ_i represent the phase shift of a wave traveling through the UC along the lattice vectors $\mathbf{d_i}$ and are given by:

$$\mu_i = \mathbf{k} \cdot \mathbf{d}_i, \tag{3}$$

with $\mathbf{k}$ the wave vector. The phase shift relationship can be represented by a matrix $\mathbf{R}$, which is function of the propagation vector $\boldsymbol{\mu}= (\mu_x, \mu_y)$ [40]. Application of the Bloch-Floquet boundary conditions leads to following eigenvalue problem:

$$\left(\mathbf{K}^{(red)} - \omega^2 \mathbf{M}^{(red)}\right) \mathbf{q}^{(red)} = \mathbf{R}^{*T}\mathbf{f} = \mathbf{0}, \tag{4}$$

with $\mathbf{K}^{(red)} = \mathbf{R}^{*T}\mathbf{K}\mathbf{R}$ and $\mathbf{M}^{(red)} = \mathbf{R}^{*T}\mathbf{M}\mathbf{R}$ the reduced stiffness and mass matrix, respectively, $\mathbf{q}^{(red)} = \mathbf{R}\mathbf{q}$ the reduced generalized displacement vector and the reduced generalized force vector $\mathbf{R}^{*T}\mathbf{f} = 0$ in absence of external forces [40].

Classically, undamped dispersion curves are calculated by solving the eigenvalue problem to real ω for imposed real propagation constants along the irreducible Brillouin contour [15]. Stop bands are identified as frequency regions where no free wave propagation is found.

3.2. Stop band limits

Since the resonators are added to the 2 mm panel, only this panel is analyzed using the earlier described method. First, the bare UC without resonant structures is studied as a benchmark. Next, the metamaterial UC with resonant structures is considered (Figure 3). The Bare UC is composed of a PMMA panel with dimensions of $30 \times 30 \times 2$ mm modeled with linear shell elements. The metamaterial UC is composed of the Bare UC, as host structure, and two resonant structures modeled using linear solid elements (Table 3). The dispersion curves are calculated along the Brillouin contour, defined in Figure 4a [41].

Table 3: FE model description of the analyzed UCs.

	Linear shells	Linear solids
Bare UC	246	-
Metamaterial UC	246	1010

In the dispersion diagram of the bare UC, three wave types are identified: bending (1), longitudinal (2) and shear (3). No stop band is present for any of the wave types (Figure 4b). In the dispersion diagram of the metamaterial UC, a resonance based stop band for the targeted flexural waves is obtained between 538 Hz and 621 Hz (Figure 4c). Two branches limit

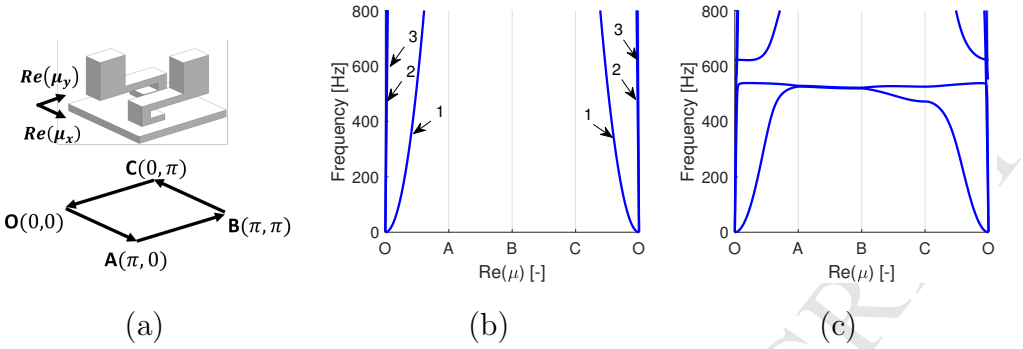

Figure 4: Along the irreducible Brillouin contour (a) the bending wave dispersion curve of the metamaterial UC (c) has a clear stop band, compared to no stop band behaviour in the bare UC dispersion curves (b).

the lower frequency of the stop band. This happens due to the presence of two resonant structures with the same tuned frequency in one UC. Therefore, two modes of the resonant structures are found at the same frequency, having in-phase and anti-phase motion (Figure 5).

4. Dynamic mass based sound transmission loss prediction

This section describes the proposed STL prediction method for a metamaterial double panel partition by combining the MRT with the metamaterial dynamic mass. First, the MRT is described. Next, the metamaterial dynamic mass is derived to incorporate the stop band effect of a UC with an arbitrary complex resonant structure in the MRT. Finally, the introduced method is used to predict the STL of the three considered double panel configurations.

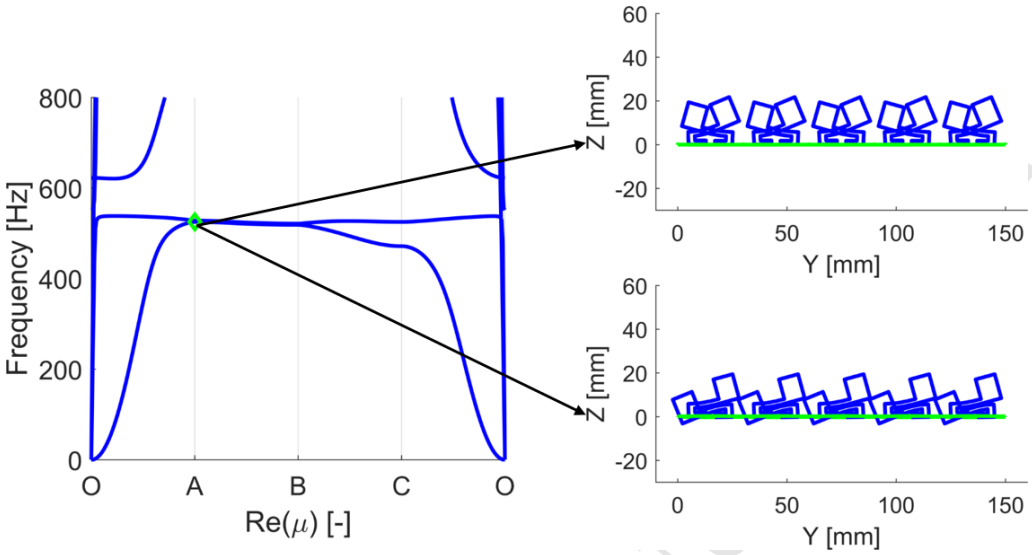

Figure 5: Visualization of the two modes of the resonant structures which limit the lower frequency of the stop band (left): in-phase (top right) and anti-phase (bottom left) motion of 5 UCs in the y-direction (Figure 4a) in the two branches.

4.1. Multiple Reflection Theory

To predict the STL of the metamaterial double panel, an infinite plate representation is used. It is known that finiteness of a partition influences the STL, because of resonant transmission due to structural modal behaviour and diffraction effects due to the finite aperture size [26]. However, in and around the stop band frequency range of interest, the STL of a locally resonant metamaterial panel was found to be in good agreement with infinite plate STL predictions, especially in presence of damping [26]. The MRT is applied for the STL calculation of the double panel configurations. This method is briefly decribed in the following, while a complete description of the method is given in [3]. The MRT considers infinite homogeneous

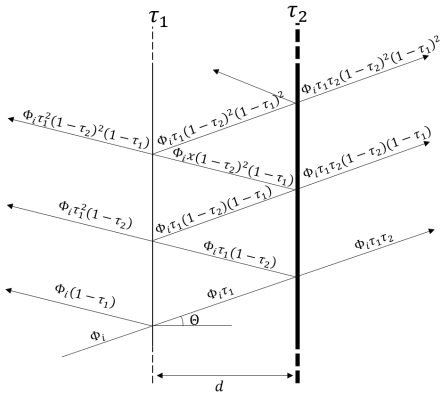

Figure 6: Acoustic ray (Φ_i) impinging in a double partition panel and being attenuated and reflected according to the acoustic mass-law of each panel (1 and 2) [3].

panels 1 and 2 constituting the double panel partition and treats the sound incident waves as rays, which are attenuated and reflected at each panel interface according to the acoustic mass law of each panel (Figure 6). Each time a ray with amplitude Φ_I impinges onto a panel, its transmitted amplitude is scaled with factor τ_i according to the acoustic mass-law of that panel:

$$\tau_i = \frac{1}{1 + \frac{j\omega m_i' \cos\theta}{2\rho_0 c_0}}, \tag{5}$$

where $i = 1, 2$ denotes the panel onto which the sound ray impinges (Figure 6), m_i' denotes the mass per area of panel i and θ is the angle of incidence. The reflected amplitude of the ray is conversely scaled by $(1 - \tau_i)$. As a transmission problem is considered, the rays emerging at the other side of the double panel partition are of importance, and the sum of these rays gives the amplitude of the transmitted wave. The transmission coefficient τ is then found as:

$$\tau = \left|\frac{\Phi_I}{\Phi_T}\right|^2 = \left|\frac{\tau_1\tau_2}{1-(1-\tau_1)(1-\tau_2)\,e^{-2jkd\cos\theta}}\right|^2, \tag{6}$$

where $e^{-2jkd\cos\theta}$ is related to the phase shift caused by the transmission and reflections in the air gap. To obtain a better agreement with measurements, a factor α is introduced, as proposed in [3]. Corresponding to the range of values reported in [3], a value of $\alpha = 0.97$ is applied in Eq. (6), which then takes the following form:

$$\tau = \left|\frac{\Phi_I}{\Phi_T}\right|^2 = \left|\frac{\tau_1\tau_2}{1-\alpha(1-\tau_1)(1-\tau_2)\,e^{-2jkd\cos\theta}}\right|^2. \tag{7}$$

To acquire the diffuse field transmission coefficient, this equation can be integrated over the angles of incidence using the Paris equation:

$$\overline{\tau}(\omega) = \frac{\int_0^{\theta_l}\tau(\omega,\theta)\cos\theta\sin\theta d\theta}{\int_0^{\theta_l}\cos\theta\sin\theta d\theta}, \tag{8}$$

where θ_l is maximum angle of incidence. In this paper, $\theta_l = 80^o$ is chosen to obtain good agreement with experimental results [3].

The classic MRT introduced in [3] relies on the acoustic mass-law, which in its turn is based on the static mass of the panels. A further extension to incorporate the stop band behavior is thus required. In what follows, the static mass is replaced by a dispersion curve based dynamic mass of the metamaterial panel. First, the dynamic mass equation is derived. Next, the dispersion curves are used to obtain the parameters required to use the derived equation of an UC with arbitrary complex resonant structure.

4.2. Dynamic mass equation

To calculate the dynamic mass of a metamaterial panel, this paper proposes to use the dynamic mass equation of a lumped 2 degree-of-freedom (DOF) system combined with the stop band limits obtained from the FE UC based dispersion curve calculations. In this way, is possible to homogenize the mass of the 2 DOF system in a 1 DOF system.

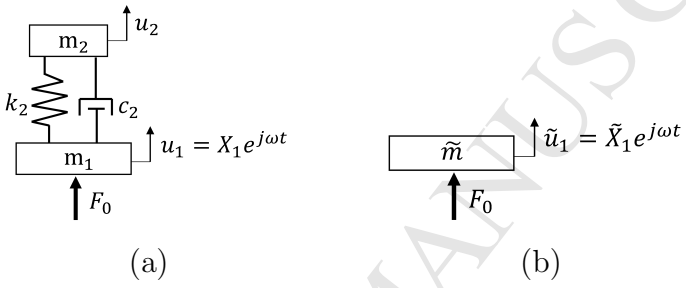

Figure 7: The 2 DOF system (a) is replaced by a 1 DOF system (b) with the equivalent dynamic mass $\tilde{m}$.

Consider the translational 2 DOF system presented in Figure 7, in which m_1 represents the UC host structure mass, to which a tuned vibration absorber with mass m_2, spring stiffness k_2 and viscous damping c_2 is attached. The host structure mass is excited by a point force F_0. The equations of motion of this system are:

$$\begin{bmatrix} m_1 & 0 \\ 0 & m_2 \end{bmatrix} \begin{Bmatrix} \ddot{u}_1 \\ \ddot{u}_2 \end{Bmatrix} + \begin{bmatrix} c_2 & -c_2 \\ -c_2 & c_2 \end{bmatrix} \begin{Bmatrix} \dot{u}_1 \\ \dot{u}_2 \end{Bmatrix} + \begin{bmatrix} k_2 & -k_2 \\ -k_2 & k_2 \end{bmatrix} \begin{Bmatrix} u_1 \\ u_2 \end{Bmatrix} = \begin{Bmatrix} F_0 \\ 0 \end{Bmatrix} \tag{9}$$

where u_i is the displacement of mass i, while $\dot{u}_i = du_i/dt$ and $\ddot{u}_i = d^2u_i/dt^2$. Assuming a time harmonic response, the displacements in Eq. (9) are writ-

ten as $u_i(t) = X_i e^{j\omega t}$. Next, X_2 is eliminated from the time harmonic equations of motion, resulting in the following transfer function between the input force F_0 and the time-harmonic displacement response X_1 of m_1:

$$\frac{X_1}{F_0} = \frac{-\omega^2 m_2 + j\omega c_2 + k_2}{(-\omega^2 m_1 + j\omega c_2 + k_2)(-\omega^2 m_2 + j\omega c_2 + k_2) - (-j\omega c_2 - k_2)^2}. \quad (10)$$

The 2 DOF system is replaced by the 1 DOF system of Figure 7b which consists of a single lumped mass $\tilde{m}$ with time harmonic displacement response $\tilde{u}_1(t) = \tilde{X}_1 e^{j\omega t}$. For this system, the transfer function between the excitation F_0 and response $\tilde{X}_1$ is:

$$\frac{\tilde{X}_1}{F_0} = \frac{1}{-\omega^2 \tilde{m}}. \quad (11)$$

By imposing equality of both transfer functions (10) and (11), and solving for $\tilde{m}$, the following equivalent mass of the 2 DOF system is obtained:

$$\frac{X_1}{F_0} = \frac{\tilde{X}_1}{F_0} \quad \Leftrightarrow \quad \tilde{m} = \frac{F_0}{-\omega^2 X_1} = m_1 + m_2 \frac{j\omega c_2 + k_2}{-\omega^2 m_2 + i\omega c_2 + k_2}. \quad (12)$$

This is re-written as follows:

$$\tilde{m} = m_1 + m_2 \left[\frac{\frac{2j\zeta_2\omega}{\omega_2} + 1}{1 + \frac{2j\zeta_2\omega}{\omega_2} - \left(\frac{\omega}{\omega_2}\right)^2} \right], \quad (13)$$

with damping ratio $\zeta_2 = c_2/2\sqrt{k_2 m_2}$ and natural frequency $\omega_2 = \sqrt{k_2/m_2}$ of the tuned vibration absorber in the 2 DOF system.

For illustration purposes, the equivalent dynamic mass $\tilde{m}$ is calculated for an undamped 2 DOF system with properties ($\zeta_2 = 0$), $m_1 = 1$ kg, $m_2 = 0.2m_1$ and $\omega_2 = 500$ Hz (Figure 8). At $\omega = 0$, the equivalent dynamic

mass equals the total static mass m_1+m_2. Towards the natural frequency ω_2 of the resonator, $\tilde{m}$ strongly increases and tends to infinity. After resonance, anti-phase motion occurs between m_1 and m_2, causing $\tilde{m}$ to assume negative values until ω_β, after which $\tilde{m}$ gradually evolves towards m_1.

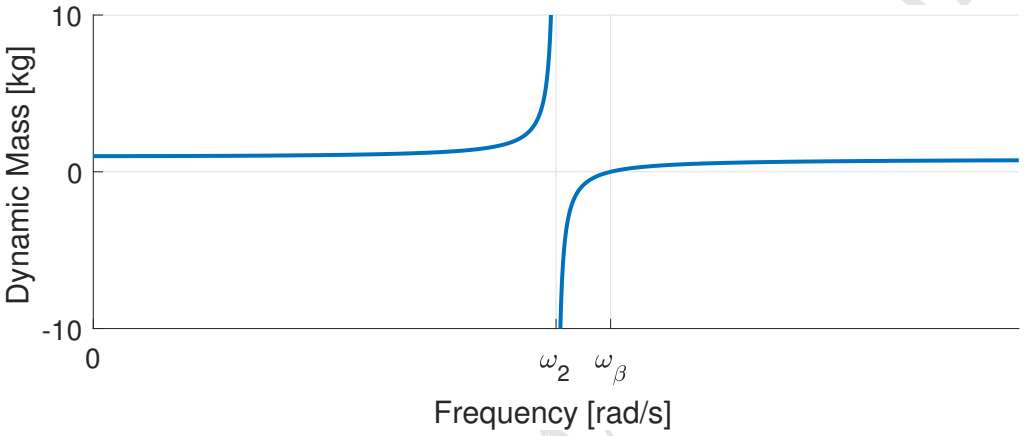

Figure 8: The equivalent dynamic mass of an undamped metamaterial system tends to ∞ when $\omega \to \omega_2$, after which it changes to negative values until ω_β.

The negative dynamic mass between ω_2 and ω_β is obtained because only the transfer function of the first DOF of the 2 DOF system is used to describe the total system response. Consequently, an observability problem is encountered, which allows $\tilde{m}$ to take negative values. The negative dynamic mass effect means that the excitation force is balanced by the inertial force exerted by the resonator, which leads to $u_1(t) = 0$ [42]. Resonance based stop bands are known to lead to to negative dynamic mass [42, 43, 44, 33]. The negative dynamic mass frequency range in locally resonant metamaterials corresponds to the stop band frequency range generated by the sub-wavelength resonant additions [43, 31].

4.3. Dynamic mass of a metamaterial

In previous subsection the equivalent dynamic mass is calculated for a 2 DOF system. However, real systems have multiple DOFs. Consequently, a simplification from a metamaterial UC to a 2 DOF system is required for the previously derived formulation to be applicable.

To calculate the dynamic mass of a given UC using Eq. (13) four parameters have to be determined: ζ_2, m_1, ω_2 and m_2. The damping ratio of the resonator ζ_2 is determined by the measured modal damping. The other three parameters are less straightforward to derive for a realizable UC containing a host structure mass m_{HS} and a possibly complex resonator with mass m_{Res} (Figure 9). Since not all resonator mass is effectively resonating, m_2 differs from m_{Res} and m_1 differs from m_{HS}. In addition, the natural frequency of the resonator depends on the stiffness of the resonator, the host structure and their connection, causing ω_2 to possibly differ from the tuned frequency of the separate resonator.

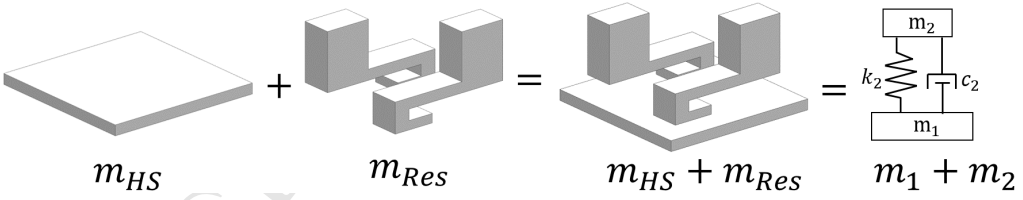

Figure 9: Masses of a realizable metamaterial UC compared to the masses of a 2 DOF system and the conservation of mass between both systems.

To determine m_1, conservation of mass is applied to the realizable metamaterial UC and the simplified 2 DOF system:

$$m_1 = m_{HS} + m_{Res} - m_2. \tag{14}$$

To determine ω_2 and m_2, the negative mass property of the metamaterial inside the SB is exploited. The lower stop band limit ω_L and the higher stop band limit ω_H obtained with the dispersion curves of the undamped metamaterial structure correspond to the limits ω_2 and ω_β of the negative mass frequency range of the equivalent system [43]:

$$\begin{aligned} \omega_2 &= \omega_L, \\ \omega_\beta &= \omega_H. \end{aligned} \tag{15}$$

By doing so, the influence on the resonance frequency of adding the resonant structures onto the host structure is accounted for. By substituting Eq. (14) into Eq. (13) and evaluating at $\omega = \omega_H$ for an undamped system, for which $\tilde{m} = 0$, m_2 is obtained:

$$m_2 = \frac{m_{HS} + m_{Res}}{1 - \frac{1}{1-\left(\frac{\omega_H}{\omega_L}\right)^2}}. \tag{16}$$

By substituting the known m_1, ω_2 and m_2 in Eq. (13), the equivalent dynamic mass of the metamaterial panel is found as follows:

$$\tilde{m} = m_{HS} + m_{Res} + \frac{m_{HS} + m_{Res}}{1 - \frac{1}{1-\left(\frac{\omega_H}{\omega_L}\right)^2}} \left[\frac{\frac{2j\zeta_2\omega}{\omega_L} + 1}{1 + \frac{2j\zeta_2\omega}{\omega_L} - \left(\frac{\omega}{\omega_L}\right)^2} - 1 \right]. \tag{17}$$

In the proposed method, damping is only considered in the resonant structure. Since damping in the host structure was found to have a negligible effect on the STL performance in and around the stop band, neglecting damping in the host structure with the current approach is not expected to affect the STL predictions, especially in and around the targeted stop band frequency range of interest [45].

The above Eq. (17) is applied to the considered metamaterial structure with the parameters listed in Table 4 to illustrate the negative dynamic mass effect (Figure 10). At $\omega = 0$, the metamaterial dynamic mass equals the equivalent static mass configuration. The dynamic mass increases towards a peak at ω_L due to the resonance based stop band induced by the sub-wavelength resonant additions. At ω_H, $\tilde{m} = 0$ indicating the end of the stop band. Furthermore, the dynamic mass of the metamaterial configuration is reduced after the stop band. Since part of the resonator is not partaking in the resonance, the dynamic mass after the stop band evolves towards a value smaller than the equivalent static mass, but greater than the original bare host structure configuration. By introducing the calculated dynamic metamaterial mass into Eq. (7) for the corresponding panel, the STL of the metamaterial double panel can be predicted.

Table 4: Parameters used to calculate the dynamic mass of the metamaterial panel.

m_{HS}	m_{Res}	ω_L	ω_H	ζ_2
2.1 g	2.0 g	536 Hz	620 Hz	2.5 %

4.4. Sound transmission loss prediction of the partitions

The normal and diffuse incidence STL are predicted for the original, equivalent static mass and metamaterial double panels using the MRT. The masses per area are shown in Table 5 for the original and equivalent mass panels. The mass per area of the metamaterial panel is obtained by dividing the dynamic mass obtained with Eq. (17) by the UC area. This homogenization is allowed since the UC dimensions are sub-wavelength [22].

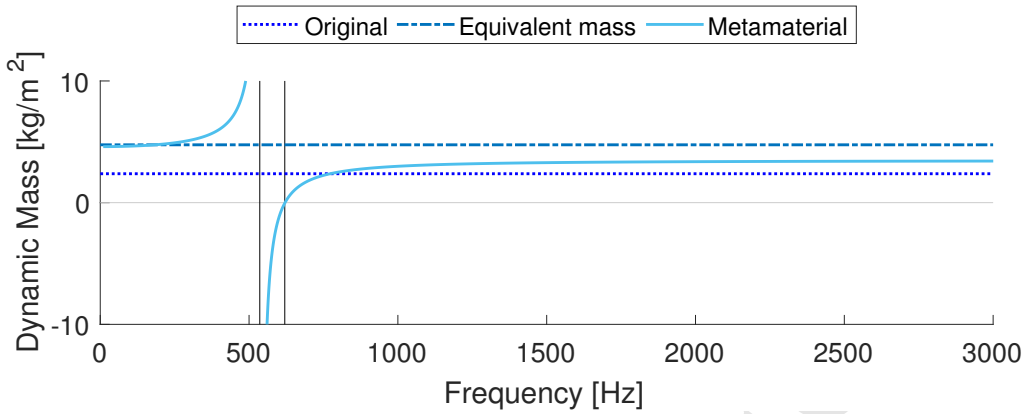

Figure 10: The metamaterial dynamic mass per area tends to ∞ at ω_L (first black vertical line) and is equal to 0 at ω_H (second black vertical line), after which it takes a value smaller than the equivalent static mass configuration and larger than the original configuration.

Table 5: Masses per area of the PMMA panels used to compose the original and equivalent mass configurations.

2 mm panel	4 mm panel
2.3768 kg/m^2	4.7535 kg/m^2

The normal and diffuse STL of the metamaterial show a strong improvement around the f_{MAM} of the original configuration due to the tuned stop band effect (Figure 11 and Figure 12). The original and equivalent mass configuration show an STL dip around their f_{MAM} for normal incidence, which becomes less outspoken for diffuse incidence. This happens because each incidence angle leads to an oblique mass-air-mass resonance at a different frequency, reducing the STL also for frequencies exceeding f_{MAM} [46, 3]. This gives origin to the upper London frequency, which is the maximum frequency at which the mass-air-mass phenomenon can occur, determined by

the maximum considered incidence angle, chosen as $\theta_l = 80°$ in this study [3].

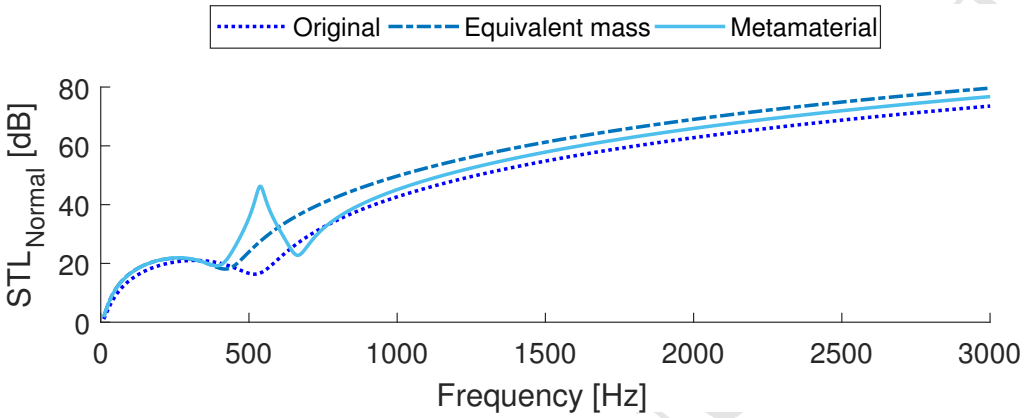

Figure 11: STL prediction for normal incidence for the three studied configurations: original, equivalent static mass and metamaterial, where a strong improvement in the mass-air-mass resonance frequency region of the original configuration is obtained with the metamaterial configuration.

Right before and after the stop band, however, the metamaterial shows a reduced STL performance, which is more pronounced in the normal STL. This can be explained by the creation of two mass-air-mass resonances by the metamaterial panel in the double panel configuration: at 409 Hz and 663 Hz. These resonances can be calculated when the dynamic mass per area of the metamaterial panel is introduced in Eq. (1). After the second mass-air-mass resonance, the predicted STL of the metamaterial panel evolves towards a value in between the original and equivalent static mass configuration, corresponding to its dynamic mass (Figure 10).

In conclusion, the locally resonant metamaterial concept shows potential to improve the STL of the double wall structure when tuned to its mass-air-mass frequency range. In the targeted frequency range, the metamaterial

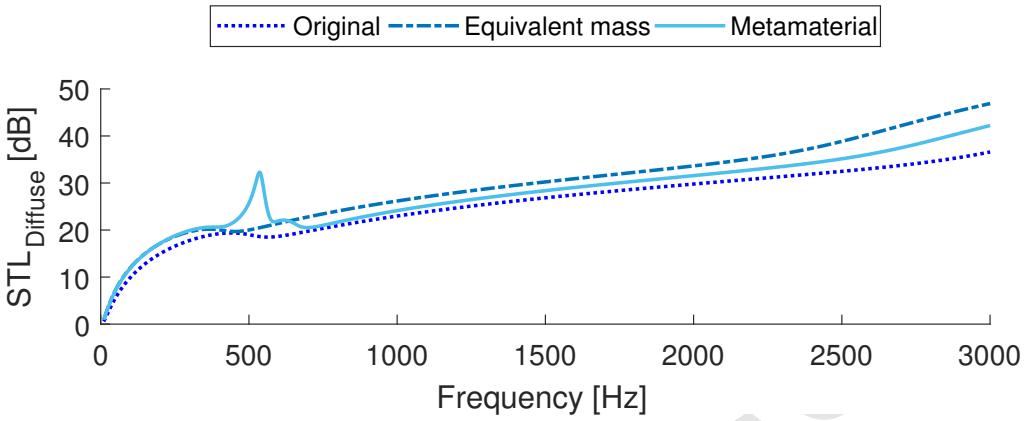

Figure 12: STL prediction for diffuse incidence for the three studied configurations: original, equivalent static mass and metamaterial, the dip in the STL due to the mass-air-mass resonance is not as pronounced as for normal incidence (Figure 11), however, the stop band effect is still clearly obtained with the metamaterial configuration.

double panel outperforms a regular mass addition by increasing the panel thickness. In section 6, the numerical predictions will be validated experimentally, after introducing the measurement setup in the following section 5.

5. Test setup

This section describes the measurement setup for the validation of the resonant structure design and the setup for the sound insertion loss (IL) measurements of the manufactured double panel configurations.

5.1. Resonant structure design validation

In order to validate the design of the resonant structures, the resonance frequency of the tuned bending mode and the corresponding modal damping ratio is measured for 10 manufactured resonant structures. The resonance

frequency is determined experimentally by gluing the resonant structure to a rigid aluminum base which is connected to a shaker (Figure 13) [7]. The Loctite®406 contact adhesive is used to glue the resonant structures, which is known from previous work to have a negligible damping influence [7, 38]. The vibration response of the resonators is measured at its end point mass using a Scanning Polytec PSV-500 Laser Doppler Vibrometer [47].

The average resonance frequency $\overline{f}$ is determined by a linear average of the identified resonance frequencies. The standard deviation is calculated as:

$$\sigma = \sqrt{\left(\frac{\sum_{i=1}^{n}\left(f_i - \overline{f}\right)^2}{n}\right)}, \tag{18}$$

where n is the number of tested resonant structures, f_i is the measured natural frequency. The modal damping of the resonator is estimated by linearly averaging the modal damping of the same 10 resonant structures, obtained by applying the half power bandwidth method [36].

5.2. Insertion loss measurements on the KU Leuven Soundbox

To validate the numerically predicted STL, the IL of realized double panel configurations is measured using a small acoustic cabin. The IL is used, since it is difficult to obtain STL measurements with the used setup. The IL differs from the STL since it also carries information about the environment in which the test is performed [48].

The small acoustic cabin used to install and test the panels is the KU Leuven Soundbox [49, 48] (Figure 14). This cavity is made of concrete walls and has an inner volume of 0.83 m^3. Its walls are skewed to obtain an

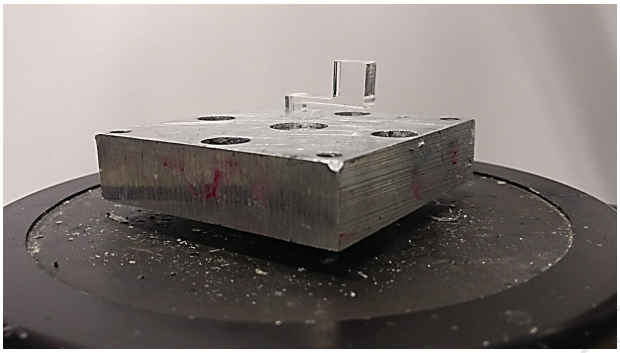

Figure 13: To measure the resonance frequency and modal damping of the resonant structure, the test sample is glued on an aluminum block, which is excited by a shaker. The response of the test sample is measured at its end point mass using a laser vibrometer, not shown in the figure.

evenly spaced frequency distribution of the acoustic modes below the field diffusivity limit at 1600 Hz [48]. The cavity is sealed by a 35 mm thick aluminum front wall, with an A2 sized aperture (420×594 mm) onto which test samples can be attached. The panels are clamped with a frame on the front wall using 52 bolts, to which a consistent 30 Nm torque is applied.

To fit the A2 aperture, the manufactured double panel partitions are composed of two PMMA panels with total dimension of 860×640 mm, as part of the panels area is used for their installation on the front wall (Figure 16). The resonant structures are added to the PMMA panel by adhesive bonding (Loctite®406). In the clamped boundary, a Medium Density Fiberboard (MDF) panel with 8 mm is used as a spacer to create the designed air gap, without covering the acoustic wetted surface (Figure 15 and Figure 16).

The IL is calculated as:

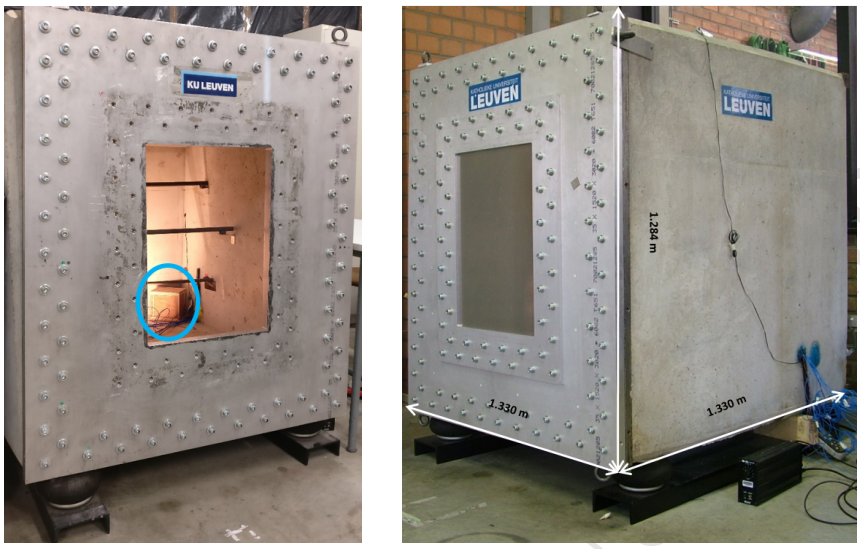

(a) (b)

Figure 14: IL measurements are performed on the KU Leuven Soundbox small cabin by acquiring the radiated sound power in open (a) and closed (b) configuration for the same acoustic excitation inside the cavity (loudspeaker, indicated by the blue circle).

$$IL\,(f) = 10\log_{10}\frac{W_{open}}{W_{closed}} \tag{19}$$

where W_{open} and W_{closed} are the measured sound powers radiated through the aperture in open configuration and closed by the test sample, respectively, when acoustically excited by a loudspeaker inside the cavity (Figure 14a). The sound power is measured using a B&K sound intensity PP probe type 2681 with a spacer of 12 mm, which allows measurements from 125 Hz to 6300 Hz [50], and a scanning measurement procedure is applied [6]. The signal is acquired by an LMS Scadas mobile coupled to LMS Test.Lab 16 software.

Since the IL carries information about the testing environment, the stop

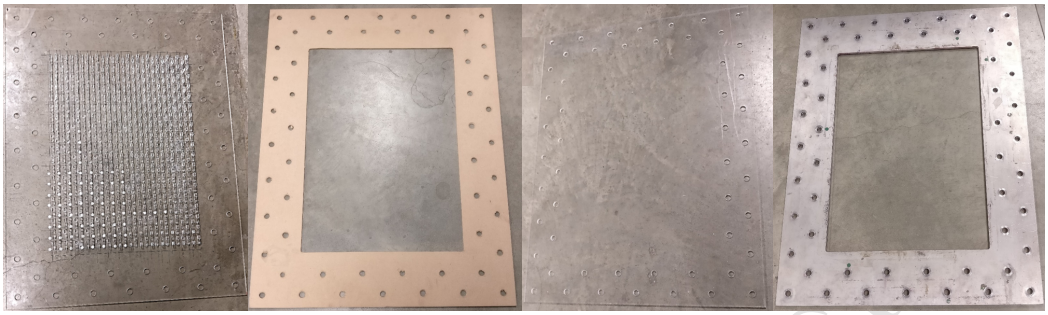

(a) (b) (c) (d)

Figure 15: The metamaterial double panel is composed of a PMMA 2 mm thick metamaterial panel (a), an MDF spacer with 8 mm of thickness (b), an bare PMMA 4 mm thick panel (c), while a 10 mm thick aluminum frame is used to clamp it on the KU Leuven Soundbox (d) as shown in Figure 16.

band effect can be shown more clearly, by calculating the difference in IL as follows:

$$\Delta IL = IL_M - IL_B \tag{20}$$

where IL_M is the narrow-band IL of the metamaterial double panel configuration and IL_B is the narrow-band IL of one of the bare configurations: original or equivalent mass. To facilitate the interpretation of the data, the IL and ΔIL are represented in 12^{th} octave frequency bands averaged format.

6. Experimental validation

This section first discusses the measured natural frequencies of the resonant structures. Next, the IL results for the three considered double panel configurations are discussed and compared to the numerical predictions to

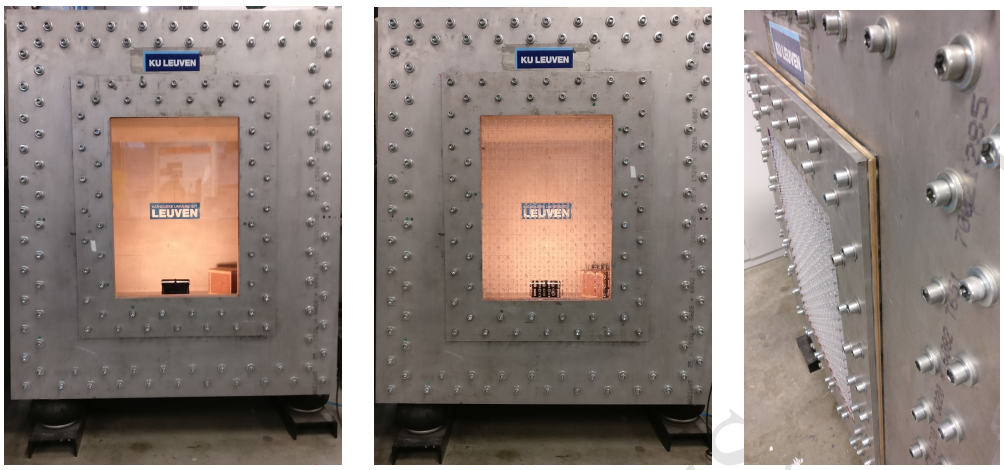

(a) (b) (c)

Figure 16: Realization of the original (a) and metamaterial (b) double panel partition, clamped on the KU Leuven Soundbox, with the MDF spacer in between (c).

demonstrate the metamaterial double panel potential. Finally, a comparison of predictions and measurements is presented using the ΔIL to validate the method proposed in this paper.

6.1. Resonant structure measurements

The numerically predicted and experimentally obtained average resonance frequencies are in good agreement (Table 6). The standard deviation on the measured resonance frequency indicates some variation, which can be explained by manufacturing imprecisions as well as slight variations in the material properties. The variation of resonance frequency breaks the periodicity assumed in the UC analysis. In [51] it was shown that variations on the resonance frequency leads to a widening of the frequency range of attenuation, but reduces the peak attenuation performance, and can be

Table 6: Comparison between numerically calculated and experimentally measured average natural frequency of the designed resonant structure.

Numerical	Experimental
562.97 Hz	562.75 ± 8.18 Hz

compared to an increase of the resonator damping. Consequently, the UC analysis can still be applied.

6.2. Insertion loss results

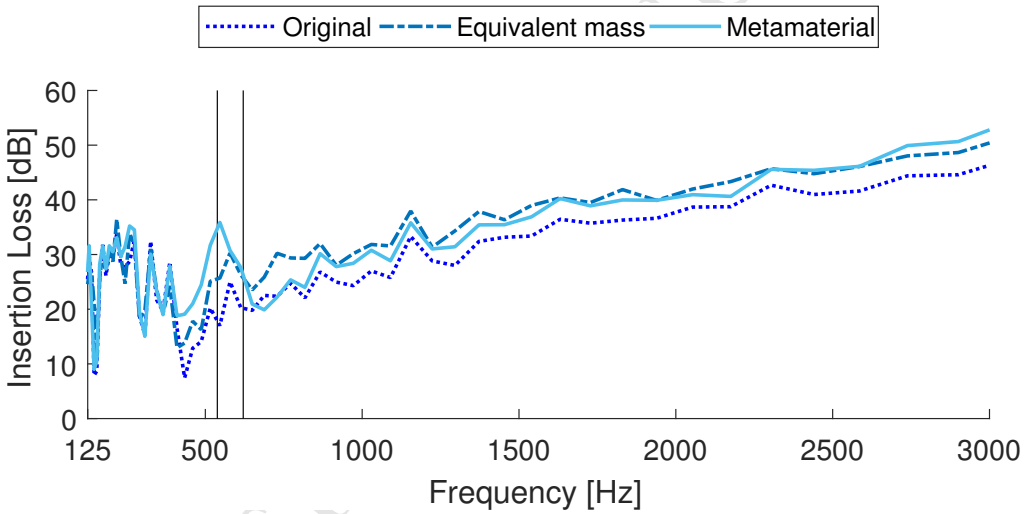

Figure 17: The measured metamaterial double partition panel IL strongly outperforms the original and equivalent static mass IL in the stop band frequency region, represented by the black vertical lines.

The metamaterial double panel outperforms both the original and equivalent static mass double panel below and inside the predicted stop band (Figure 17). The metamaterial is outperformed by both bare double panel configurations near the upper limit of the stop band. This is caused by the

low dynamic mass and the introduced second mass-air-mass resonance, as discussed in section 4.4. Around 1000 Hz the metamaterial configuration reaches a similar IL performance as the equivalent static mass configuration. This behavior corresponds well to the predictions for the normal incidence with the proposed MRT method (Figure 11). However, direct comparison of the absolute predicted STL and measured IL shows overestimation when normal incidence is considered (Fig. 11) and underestimation when diffuse field (Fig. 12) is considered. This is explained by the mass-air-mass resonance frequency range being below the field diffusivity limit of the KU Leuven Soundbox, as well as the intrinsic difference between STL and IL, with the latter containing information of the measurement setup.

In the measured IL of the original configuration, a pronounced dip is measured at 444 Hz, which does not correspond to the predicted mass-air-mass resonance frequency of 532.9 Hz. This IL dip is related to the presence of 7 acoustic modes of the Soundbox cavity in the $400 - 500$ Hz frequency range [48]. To verify the effect of these modes, the IL is measured using the panels of the original configuration with an air gap of 4 mm and a predicted mass-air-mass resonance frequency of 753.6 Hz. A dip in the IL for the 4 mm air gap configuration is found around the predicted mass-air-mass resonance frequency range. However, an IL dip around 444 Hz is also found as was the case for the 8 mm air gap (Figure 18), confirming the influence of the acoustic cavity modes on the measured IL.

In summary, the experimental IL measurements indicate an improvement around the targeted mass-air-mass resonance frequency range, as expected using the numerical predictions.

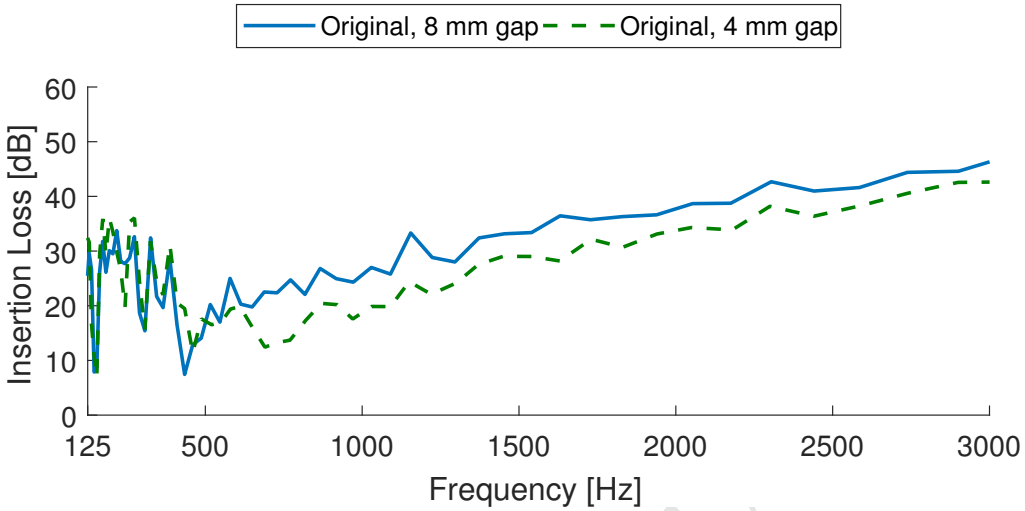

Figure 18: The IL of the bare double panel partition shows a dip at 444 Hz for both air gapscaused by acoustic modes of the KU Leuven Soundbox cavity, despite different mass-air-mass resonance frequencies at 532.9 Hz (8 mm air gap) and 753.6 Hz (4 mm air gap).

6.3. Numerical model validation

To verify the accuracy of the numerical STL predictions with the proposed extension of the MRT method, the numerically predicted STL is compared with the experimentally measured IL. The ΔIL of Eq. (20) is used to reduce the influence of the cavity and panels modes and sound incidence angles on the IL results, since the STL predictions with the extended MRT method do not carry information about the testing environment and finiteness of the panel. As discussed in section 4.1, the finite panel dimensions are expected to be of limited influence in and around the stop band frequency range, especially considering the high intrinsic damping of the PMMA material.

The normal incidence ΔSTL prediction agrees overall well with the mea-

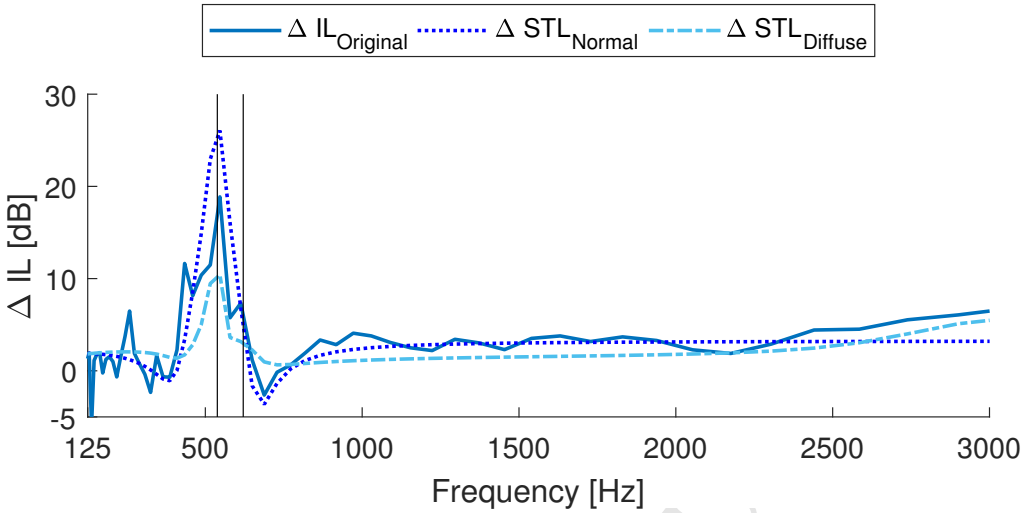

Figure 19: The calculated ΔSTL between original and metamaterial configuration for normal incidence corresponds well to the measured ΔIL. The calculated ΔSTL for diffuse field underestimates the stop band effect. Furthermore, a clear peak in the measured IL can be noticed in the stop band frequency region, represented by the vertical black lines.

sured ΔIL (Figure 19 and 20). As only normal incidence and no variability in the resonant structure is accounted for in the UC analysis based MRT calculations, the predicted normal incidence ΔSTL overestimates the peak performance. The diffuse field ΔSTL prediction, on the other hand, underestimates the peak performance found with the ΔIL obtained from the comparison with both the original and equivalent static mass double panels.

After the stop band, the severity of the measured ΔIL dip following from the additional mass-air-mass resonance is slightly overestimated by the normal incidence ΔSTL prediction, but more strongly overestimated with the diffuse field ΔSTL prediction. The stronger deviation of the diffuse field ΔSTL prediction is explained by the occurrence of the oblique mass-air-mass resonance in infinite double panel partitions as discussed earlier in

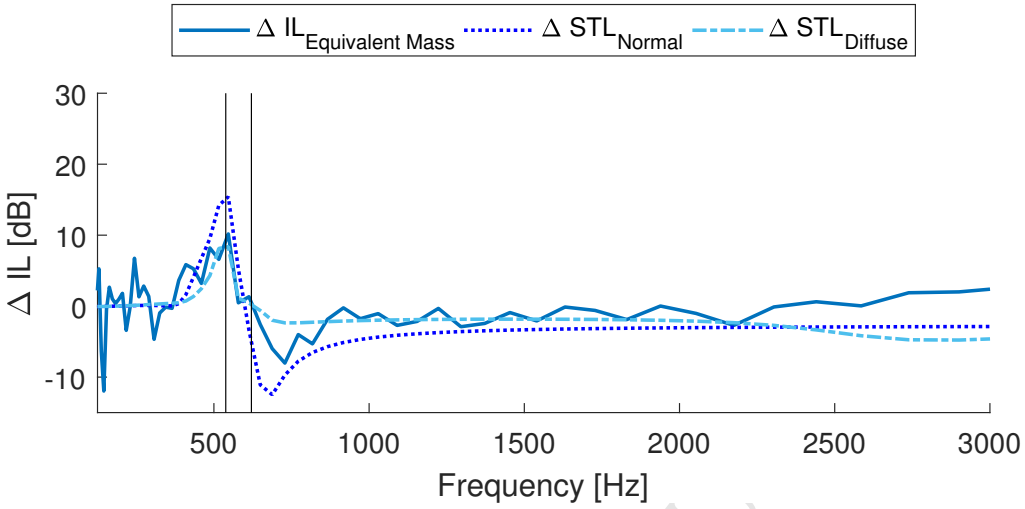

Figure 20: The stop band effect is clearly present in the ΔIL between the metamaterial and equivalent static mass configuration. The ΔSTL between original and metamaterial configuration for normal incidence again corresponds well to the measured ΔIL. The ΔSTL for diffuse field does not predict the reduced acoustic insulation performance measured after the stop band frequency region, represented by the black vertical lines.

section 4.4. Moreover, the acoustic field inside the KU Leuven Soundbox for the targeted frequency range is neither normal nor diffuse, resulting in the measured results lying in between both normal and diffuse field predictions. For the given test setup and samples, a better agreement is found between normal ΔSTL predictions and ΔIL measurements.

To summarize, the measured ΔIL highlights the stop band effect obtained with the metamaterial double panel as a strong improvement of the acoustic insulation performance in the targeted mass-air-mass frequency region compared to both bare configurations. From the good agreement between measurements and predictions, it can be concluded that the proposed STL prediction method allows a fast and indicative calculation to assess the stop band effect obtained by the use of complex resonant structures.

7. Conclusion

In this work, a realizable metamaterial double panel is presented to improve the acoustic insulation performance of a double panel in the mass-air-mass resonance frequency range. To design the metamaterial double panel, an extension of the MRT method with the finite element unit cell analysis based dynamic metamaterial mass is proposed, to allow for simple and fast STL predictions that can account for complex resonator designs.

The numerical predictions indicate the potential of the metamaterial double panel as a lightweight solution, since a strong STL improvement is predicted around the targeted mass-air-mass resonance frequency range. To validate the metamaterial potential as well as the applicability of the proposed STL prediction method, a metamaterial double panel is manufactured and its acoustic insulation performance is measured on a small acoustic cabin. Good agreement is obtained between numerically predicted ΔSTL and experimentally measured ΔIL, comparing the metamaterial double panel against the original bare double panel as well as against the equivalent static mass double panel configuration. It is concluded that the proposed approach is a powerful tool in a design phase to assess the stop band effect related acoustic insulation improvements for metamaterial double panels with realizable resonators.

Acknowledgments

The research of N. F. Melo is funded by a PhD Scholarship Sciences without Borders CNPq Brazil (201414/ 2014-7). The research of L. Van Belle is funded by a grant from the Research Foundation - Flanders (F.W.O.). Elke

Deckers is a postdoctoral researcher of the Research Foundation - Flanders (F.W.O.). This research was partially supported by Flanders Make, the strategic research centre for the manufacturing industry.

References

[1] F. J. Fahy, Sound and structural vibration: radiation, transmission and response, Academic press, 2012.

[2] J. Quirt, Sound transmission through windows i. single and double glazing, The Journal of the Acoustical Society of America 72 (3) (1982) 834–844.

[3] K. Mulholland, H. Parbrook, A. Cummings, The transmission loss of double panels, Journal of Sound and Vibration 6 (3) (1967) 324–334.

[4] F. Xin, T. Lu, C. Chen, Vibroacoustic behavior of clamp mounted double-panel partition with enclosure air cavity, The Journal of the Acoustical Society of America 124 (6) (2008) 3604–3612.

[5] C. Claeys, K. Vergote, P. Sas, W. Desmet, On the potential of tuned resonators to obtain low-frequency vibrational stop bands in periodic panels, Journal of Sound and Vibration 332 (6) (2013) 1418–1436.

[6] C. Claeys, E. Deckers, B. Pluymers, W. Desmet, A lightweight vibro-acoustic metamaterial demonstrator: Numerical and experimental investigation, Mechanical Systems and Signal Processing 70 (2016) 853–880.

[7] C. Claeys, N. G. R. de Melo Filho, L. Van Belle, E. Deckers, W. Desmet, Design and validation of metamaterials for multiple structural stop bands in waveguides, Extreme Mechanics Letters 12 (2017) 7–22.

[8] P. Sheng, X. Zhang, Z. Liu, C. Chan, Locally resonant sonic materials, Physica B: Condensed Matter 338 (1) (2003) 201–205.

[9] J. H. Oh, H. M. Seung, Y. Y. Kim, Adjoining of negative stiffness and negative density bands in an elastic metamaterial, Applied Physics Letters 108 (9) (2016) 093501.

[10] T. Wang, M.-P. Sheng, Z.-W. Guo, Q.-H. Qin, Flexural wave suppression by an acoustic metamaterial plate, Applied Acoustics 114 (2016) 118–124.

[11] P. F. Pai, Metamaterial-based broadband elastic wave absorber, Journal of Intelligent Material Systems and Structures 21 (5) (2010) 517–528.

[12] D. Beli, J. Arruda, M. Ruzzene, Wave propagation in elastic metamaterial beams and plates with interconnected resonators, International Journal of Solids and Structures 139 (2018) 105–120.

[13] X. Zhou, X. Liu, G. Hu, Elastic metamaterials with local resonances: an overview, Theoretical and Applied Mechanics Letters 2 (4) (2012) 041001.

[14] C. Goffaux, J. Sánchez-Dehesa, A. Yeyati, P. Lambin, A. Khelif, J. Vasseur, B. Djafari-Rouhani, Evidence of fano-like interference phenomena in locally resonant materials, Physical Review Letters 88 (22). doi:10.1103/physrevlett.88.225502. URL http://dx.doi.org/10.1103/PhysRevLett.88.225502

[15] L. Brillouin, Wave propagation in periodic structures, 2nd Edition, McGraw-Hill Book Company, 1946.

[16] D. Mead, Wave propagation in continuous periodic structures: research contributions from southampton, 1964–1995, Journal of Sound and Vibration 190 (3) (1996) 495–524.

[17] B. R. Mace, D. Duhamel, M. J. Brennan, L. Hinke, Finite element prediction of wave motion in structural waveguides, The Journal of the Acoustical Society of America 117 (5) (2005) 2835–2843.

[18] D. Chronopoulos, I. Antoniadis, T. Ampatzidis, Enhanced acoustic insulation properties of composite metamaterials having embedded negative stiffness inclusions, Extreme Mechanics Letters 12 (2017) 48–54.

[19] V. Cotoni, R. Langley, P. Shorter, A statistical energy analysis subsystem formulation using finite element and periodic structure theory, Journal of Sound and Vibration 318 (4-5) (2008) 1077–1108.

[20] Y. Xiao, J. Wen, X. Wen, Sound transmission loss of metamaterial-based thin plates with multiple subwavelength arrays of attached resonators, Journal of Sound and Vibration 331 (25) (2012) 5408–5423.

[21] S. Hettler, Vibroacoustic behaviour of sandwich structures with spatially distributed resonators, Ph.D. thesis, Universitt Stuttgart (01 2013).

[22] M. Oudich, X. Zhou, M. B. Assouar, General analytical approach for sound trans-

mission loss analysis through a thick metamaterial plate, Journal of Applied Physics 116 (19) (2014) 193509.

[23] A. Hall, E. Calius, G. Dodd, K. Chan, Development of locally resonant structures for sonic barriers, in: Health Monitoring of Structural and Biological Systems 2013, Vol. 8695, International Society for Optics and Photonics, 2013, p. 86953M.

[24] J. Li, S. Li, Sound transmission through metamaterial-based double-panel structures with poroelastic cores, Acta Acustica united with Acustica 103 (5) (2017) 869–884.

[25] E. Deckers, S. Jonckheere, L. Van Belle, C. Claeys, W. Desmet, Prediction of transmission, reflection and absorption coefficients of periodic structures using a hybrid wave based–finite element unit cell method, Journal of Computational Physics 356 (2018) 282–302.

[26] L. Van Belle, C. Claeys, E. Deckers, W. Desmet, Influence of damping on the sound insulation of infinite and finite locally resonant metamaterial plates, in: Proceedings of ISMA2018 International Conference on Noise and Vibration Engineering and USD2018 International Conference on Uncertainty in Structural Dynamics, 2018.

[27] J. Yang, J. S. Lee, Y. Y. Kim, Metaporous layer to overcome the thickness constraint for broadband sound absorption, Journal of Applied Physics 117 (17) (2015) 174903.

[28] B. Assouar, M. Oudich, X. Zhou, Acoustic metamaterials for sound mitigation, Comptes Rendus Physique 17 (5) (2016) 524–532.

[29] V. Hongisto, Sound insulation of double panels-comparison of existing prediction models, Acta acustica united with acustica 92 (1) (2006) 61–78.

[30] P. Li, S. Yao, X. Zhou, G. Huang, G. Hu, Effective medium theory of thin-plate acoustic metamaterials, The Journal of the Acoustical Society of America 135 (4) (2014) 1844–1852.

[31] J. Park, B. Park, D. Kim, J. Park, Determination of effective mass density and modulus for resonant metamaterials, The Journal of the Acoustical Society of America 132 (4) (2012) 2793–2799.

[32] S. Yao, X. Zhou, G. Hu, Experimental study on negative effective mass in a 1d mass–spring system, New Journal of Physics 10 (4) (2008) 043020.

[33] P. Sheng, J. Mei, Z. Liu, W. Wen, Dynamic mass density and acoustic metamaterials, Physica B: Condensed Matter 394 (2) (2007) 256–261.

[34] N. G. Rocha de Melo Filho, L. Van Belle, C. Claeys, E. Deckers, W. Desmet, On the use of the dynamic mass of metamaterials to calculate the transmission loss based on the acoustic mass law, in: 13th International Conference on Theoretical and Computational Acoustics, Vienna, 2017.

[35] W. Heylen, S. Lemmens, P. Sas, Modal analysis theory and testing, KU Leuven, PMA division, 2014.

[36] B. A. Olmos, J. M. Roesset, Evaluation of the half-power bandwidth method to estimate damping in systems without real modes, Earthquake Engineering & Structural Dynamics 39 (14) (2010) 1671–1686.

[37] G. Wang, X. Wen, J. Wen, L. Shao, Y. Liu, Two-dimensional locally resonant phononic crystals with binary structures, Physical review letters 93 (15) (2004) 154302.

[38] L. Van Belle, C. Claeys, E. Deckers, W. Desmet, On the impact of damping on the dispersion curves of a locally resonant metamaterial: Modelling and experimental validation, Journal of Sound and Vibration 409 (2017) 1–23.

[39] L. Sangiuliano, C. Claeys, E. Deckers, B. Pluymers, et al., Force isolation by locally resonant metamaterials to reduce nvh, SAE Technical Paper (2018) 01–1544.

[40] R. Langley, A note on the force boundary conditions for two-dimensional periodic structures with corner freedoms, Journal of Sound and Vibration 167 (2) (1993) 377–381.

[41] F. Maurin, C. Claeys, L. Van Belle, W. Desmet, Finding the minimal unit cell–bloch theorem for structures with translation and reflection or rotation symmetries, Innovations in Wave Modelling location:Nottingham date:12-14 July.

[42] P. F. Pai, H. Peng, S. Jiang, Acoustic metamaterial beams based on multi-frequency vibration absorbers, International Journal of Mechanical Sciences 79 (2014) 195–205.

[43] C. Sugino, Y. Xia, S. Leadenham, M. Ruzzene, A. Erturk, A general theory for bandgap estimation in locally resonant metastructures, Journal of Sound and Vibration 406 (2017) 104–123.

[44] Y. Cheng, J. Xu, X. Liu, One-dimensional structured ultrasonic metamaterials with simultaneously negative dynamic density and modulus, Physical Review B 77 (4) (2008) 045134.

[45] L. Van Belle, E. Deckers, C. Claeys, W. Desmet, Sound transmission loss of a locally resonant metamaterial using the hybrid wave based-finite element unit cell method, in: 11th International Congress on Engineered Material Platforms for Novel Wave Phenomena-Metamaterials 2017, Marseille, France, 2017, pp. pp. 364–366.

[46] A. London, Transmission of reverberant sound through double walls, The journal of the acoustical society of America 22 (2) (1950) 270–279.

[47] Polytec GmbH PSV-500 Scanning Vibrometer Datasheet, 2016.
URL https://www.polytec.com/us/vibrometry/products/full-field-vibrometers/psv-500-scanning-vibrometer/

[48] M. Vivolo, Vibro-acoustic characterization of lightweight panels by using a small cabin, Ph.D. thesis, PhD Thesis, Arenberg Doctoral School, University of Leuven (2013).

[49] M. Vivolo, B. Pluymers, D. Vandepitte, W. Desmet, Vibro-acoustic study of lightweight components based on a new experimental setup, in: 18th International Congress on Sound and Vibration, (ICSV2011). Rio de Janeiro, Brasil. 10-14 July, 2011.

[50] B. . Kjaer, Sound Intensity (br0476), DK-2850 Naerum, Denmark (Revision Spetember 1993).
URL https://www.bksv.com/doc/br0476.pdf

[51] C. Claeys, Design and analysis of resonant metamaterials for acoustic insulation (ontwerp en analyse van resonante metamaterialen voor geluidsisolatie), Ph.D. thesis, KU Leuven Faculty of Engineering Science, Arenberg Doctoral School (April 2014).

Highlights

- Double panel STL is enhanced at the mass-air-mass frequency using locally resonant metamaterials
- A unit cell based dynamic mass calculation based on the dispersion curves is proposed
- Fast STL prediction method is proposed using the multiple reflection theory combined with the dynamic mass
- A transparent metamaterial double panel partition is designed, manufactured and tested experimentally
- Good agreement between proposed method and experimental results